ADVANCED FUNCTIONAL MATERIALS
www.afm-journal.de

Check for updates

High-Performance Organic Electrochemical Transistors and Neuromorphic Devices Comprising Naphthalenediimide-Dialkoxybithiazole Copolymers Bearing Glycol Ether Pendant Groups

Yanxi Zhang, Gang Ye, Tom P. A. van der Pol, Jingjing Dong, Eveline R. W. van Doremaele, Imke Krauhausen, Yuru Liu, Paschalis Gkoupidenis, Giuseppe Portale, Jun Song,* Ryan C. Chiechi, and Yoeri van de Burgt**

Organic electrochemical transistors (OECTs) have emerged as building blocks for low power circuits, biosensors, and neuromorphic computing. While p-type polymer materials for OECTs are well developed, the choice of high-performance n-type polymers is limited, despite being essential for cation and metabolite biosensors, and crucial for constructing complementary circuits. N-type conjugated polymers that have efficient ion-to-electron transduction are highly desired for electrochemical applications. In this contribution, three non-fused, planar naphthalenediimide (NDI)-dialkoxybithiazole (2Tz) copolymers, which systematically increase the amount of polar tri(ethylene glycol) (TEG) side chains: PNDI2OD-2Tz (0 TEG), PNDIODTEG-2Tz (1 TEG), PNDI2TEG-2Tz (2 TEG), are reported. It is demonstrated that the OECT performance increases with the number of TEG side chains resulting from the progressively higher hydrophilicity and larger electron affinities. Benefiting from the high electron mobility, excellent ion conduction capability, efficient ion-to-electron transduction, and low-lying lowest unoccupied molecular orbital energy level, the 2 TEG polymer achieves close to 10^5 on-off ratio, fast switching, 1000 stable operation cycles in aqueous electrolyte, and has a long shelf life. Moreover, the higher number TEG chain substituted polymer exhibits good conductance state retention over two orders of magnitudes in electrochemical resistive random-access memory devices, highlighting its potential for neuromorphic computing.

1. Introduction

Organic electrochemical transistors (OECTs) are ion-gated devices operated by modulating the bulk conductivity of organic (semi)conductors.[1] This electrochemical doping process allows OECTs to operate at low voltage (<1 V) and achieve high transconductance,[2] key features and advantages of OECTs compared with field-effect transistors. OECTs are ideal devices for a wide variety of applications, including printed logic circuitry,[3] bioelectronics,[4] neural signal recording,[5] and neuromorphic computing.[6,7] The active OECT channel material is an organic mixed ionic-electronic conductor (OMIEC), which effectively transports and couples ionic and electronic charges.[8] To develop high-performance OMIECs, it is crucial to understand the structure-properties relationship of the polymers in all aspects of molecular engineering, such as backbone, side chains, and substituents on the molecular structures.[9] Biological applications require stable OECT operation in aqueous

Y. Zhang, E. R. W. van Doremaele, I. Krauhausen, Y. van de Burgt
Microsystems
Department of Mechanical Engineering and Institute for Complex Molecular Systems
Eindhoven University of Technology
MB 5600 Eindhoven, The Netherlands
E-mail: y.b.v.d.burgt@tue.nl

The ORCID identification number(s) for the author(s) of this article can be found under https://doi.org/10.1002/adfm.202201593.

© 2022 The Authors. Advanced Functional Materials published by Wiley-VCH GmbH. This is an open access article under the terms of the Creative Commons Attribution License, which permits use, distribution and reproduction in any medium, provided the original work is properly cited.

DOI: 10.1002/adfm.202201593

G. Ye, J. Song
Center for Biomedical Optics and Photonics (CBOP) & College of Physics and Optoelectronic Engineering
Key Laboratory of Optoelectronic Devices and Systems
Shenzhen University
Shenzhen 518060, P. R. China
E-mail: g.ye0612@szu.edu.cn; songjun@szu.edu.cn

G. Ye, Y. Liu, R. C. Chiechi
Stratingh Institute for Chemistry
University of Groningen
AG 9747 Groningen, The Netherlands

T. P. A. van der Pol
Molecular Materials and Nanosystems
Department of Chemical Engineering and Chemistry and Institute of Complex Molecular Systems
Eindhoven University of Technology
P.O. Box 513, MB 5600 Eindhoven, The Netherlands

environments, which means that water and oxygen should not deteriorate the organic semiconductors/conductors under electrical stress. During device operation, ions migrate from the aqueous electrolyte into the polymer thin films driven by a gate voltage, followed by electrochemically doping/de-doping of the polymers resulting in the modulation of the bulk conductivity. Organic p-type semiconducting/conducting polymers, which conduct holes, have been studied intensively,[10] including the widely used commercial conducting polymer poly(3,4-ethylened ioxythiophene):poly(styrenesulfonate) (PEDOT:PSS). The development of n-type semiconducting polymers has been driven by the expansion of organic electronic applications as they are indispensable components combined with p-type materials for complementary logical circuits and energy storage.[11] Moreover, n-type semiconductors are essential for enhancement-mode biosensors for anions and metabolites.[12]

The molecular design strategy for OECT channel materials revolves around improving the ion-to-electron transduction between semiconductor and electrolyte, which is usually referred to as the OECT transconductance $g_m (g_m = \partial I_d / \partial V_G = \frac{Wd}{L} \mu C^* (V_g - V_{Th})$, which is proportional to μC^*. Here, μ is the charge carrier mobility and C^* is the volumetric capacitance. Ordinary n-type conjugated polymers cannot be directly applied to aqueous electrolyte-gated OECTs due to the low ion transport into and throughout the film. This incompatibility is ostensibly due to the hydrophobic (alkyl) side chains that are commonly used to impart solubility in organic solvents and are not an intrinsic property of n-type polymer backbones. To test this hypothesis, we replaced the hydrophobic side chains with hydrophilic polar tri(ethylene glycol) (TEG). TEG substituted naphthalenediimide (NDI)-bithiophene (2T) conjugated polymers have previously been shown to function in n-type OECTs.[13] On the other hand, a follow-up study revealed that the electron mobility of that NDI-2T based polymer drops significantly from 0.132 to 0.00184 $cm^2 V^{-1} s^{-1}$ as the fraction of glycol chains (to alkyl chains) increases.[14] Moreover, the localization of charge carriers leads to the low electron mobility of NDI-2T donor-acceptor type conjugated polymer.[15,16] Flexible polymer backbones exacerbate this problem by distorting in response to the intercalation of ions.[17] It is thus challenging to design a polymer that exhibits both high ionic and electronic mobility across a useful range of ionic doping levels. At the same time, the retention of a highly ordered crystalline structure during ionic doping is ideal for high-performance OECTs by retaining a high mobility μ as well as high volumetric capacitance C^*. For example, the OECT performance of the NDI-2T based polymer P-90 has been further improved via solvent engineering to increase crystallinity.[18] It has been demonstrated that the fused, electron-deficient ladder-type polymer, poly(benzimidazobenzophenanthroline) (BBL), not only has a highly planar and rigid backbone but also has highly delocalized charge carriers,[19] performs well in n-type OECTs.[20] Based on this concept, polymers with highly planar and rigid backbones, such as the fully-fused, electron-deficient lactam-based PgNaN[21] and fused bithiophene imide dimer-based f-BTI2TEG-FT,[22] have been developed to enhance charge mobility.

Although fused conjugated polymers have achieved significant progress, they have a synthetically-limited library that makes it increasingly difficult to develop better materials for n-type OECT to match the high performance of their p-type counterparts. There are more choices for building blocks to construct non-fused conjugated polymers, but they must be designed carefully to avoid localizing carriers and attenuating mobility. It is possible to approach the coplanar and rigid polymer backbones by manipulating intramolecular interactions (such as S–O interaction and F–H bonding).[23] Moreover, TEG side chains favor dense molecular packing with decreased π–π stacking distances in diketopyrrolopyrrole (DPP) based polymers.[24] Hence, we propose that non-fused n-type planar and rigid conjugated polymers accompanying TEG side chains can simultaneously realize high ion transport capability as well as electron mobility for electrochemical applications.

In this contribution, we investigate non-fused planar naphthalenediimide (NDI)-dialkoxybithiazole (2Tz) based copolymers for electrochemical applications (shown in **Figure 1**). We opt to control the density of the polar tri(ethylene glycol) (TEG) side chains to achieve high electron mobility and ion penetration capability simultaneously. Owing to the high planarity and rigidity of the backbone and higher density of TEG chains, conjugated polymer PNDI2TEG-2Tz (2 TEG) led to n-type OECTs achieving a high μ_e of 3.16×10^{-3} $cm^2 V^{-1} s^{-1}$, a good C^* of 367 Fcm^{-3}, and high μC^* 1.16 $Fcm^{-1} V^{-1} s^{-1}$, close to 10^5 on-off ratio, fast switching (within 0.1 s), 1000 stable operation cycles in aqueous electrolyte, and long shelf life. Moreover, PNDI2TEG-2Tz (2 TEG) and PNDIODTEG-2Tz (1 TEG) also exhibit p-type performance due to their matched energy levels. We also developed OECT based complementary inverters with a maximum gain of 23.4. Notably, PNDI2TEG-2Tz (2 TEG) exhibits good conductance state retention over 2 orders of magnitudes in electrochemical resistive random-access memory devices (EC-RAMs), highlighting its potential for neuromorphic computing. This work demonstrates that non-fused donor-acceptor conjugated polymer can achieve high electron mobility and ion penetration capability simultaneously for OECT. And it contributes to a deep understanding of the relationship between the polymer structures and the n-type OECT performance, which opens a window to design high-performance n-type OECT materials.

2. Results and Discussion

2.1. Molecular Design and Characterization

N-type conjugated polymers that simultaneously have high electron mobility and efficient ion transport properties are

J. Dong, G. Portale
Zernike Institute for Advanced Materials
University of Groningen
AG 9747 Groningen, Netherlands
I. Krauhausen, P. Gkoupidenis
Department of Molecular Electronics
Max Planck Institute for Polymer Research
55128 Mainz, Germany
R. C. Chiechi
Department of Chemistry
North Carolina State University
Raleigh, NC 27695, USA

© 2022 The Authors. Advanced Functional Materials published by Wiley-VCH GmbH

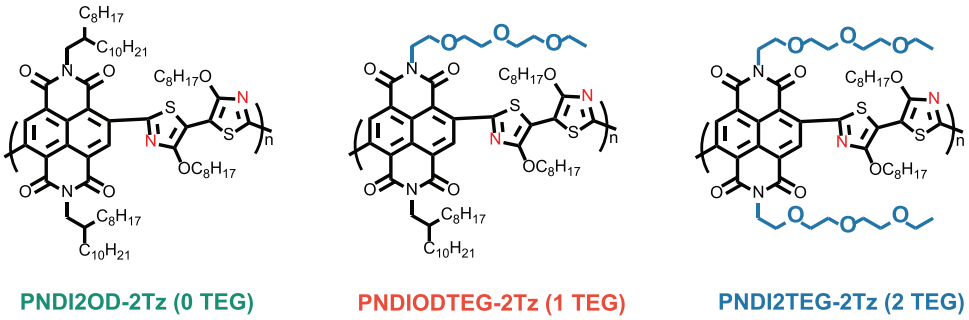

Figure 1. Chemical structures of NDI-2Tz based D–A copolymers with different substituted EG side chains: PNDI2OD-2Tz (0 TEG), PNDIODTEG-2Tz (1 TEG) and PNDI2TEG-2Tz (2 TEG).

highly desired and are ideal candidates for channel materials in OECTs. Generally, the mobility of conjugated polymers is governed by the backbone that controls the electronic structure.[25–28] Previous research has demonstrated that incorporation of hydrophilic TEG side chains onto the conjugated backbone can enhance the aqueous ions uptake and transport.[8,29–32] A rational combination of a proper conjugated backbone and TEG side chain could achieve both high electron mobility and efficient ion transport properties.

NDI-2T based conjugated polymers have been demonstrated to have a planar and rigid backbone due to the reduced steric repulsions between bithiazole and the adjacent NDI core. In addition, the electron-deficient nature of bithiazole enhances the polymer electron affinity which would be beneficial for electrochemical doping and charge carrier mobility.[33,34]

Figure 1 shows the chemical structures of non-fused NDI-2Tz copolymers: PNDI2OD-2Tz (abbreviated as 0 TEG), PNDIODTEG-2Tz (abbreviated as 1 TEG), and PNDI2TEG-2Tz (abbreviated as 2 TEG). The density functional theory (DFT)-optimized geometries are shown in Figure S11 (Supporting Information). The corresponding monomers and polymers synthetic route and synthesis details can be found in the supporting information (Figures S1 and S5, Supporting Information). The NDI-2Tz based polymers were synthesized by a palladium-catalyzed typical Stille cross-coupling polymerization of dibromo-NDI based monomers with distannyl-alkoxybithiazole based monomer after refluxing the polymerization mixture for three days. After polymerization, the resulting polymers were purified and low-molecular-weight fractions were removed by successive Soxhlet extraction with methanol and hexane. The purified high-molecular-weight polymers were extracted with chloroform, precipitated in methanol, and further dried under vacuum. The relative molecular weights M_n, M_w and polydispersity (PDI) of these three NDI-2Tz based polymers were determined by high-temperature gel permeation chromatography (GPC) analysis against polystyrene standards using trichlorobenzene as the eluent at 150 °C. The resulting data are shown in Figure S6 (Supporting Information). Their chemical structures were characterized by H NMR (Figure S7, Supporting Information) and FT-IR (Figure S8, Supporting Information).

The thermal properties of these three NDI-2Tz based conjugated polymers were evaluated by thermogravimetric analysis (TGA) and differential scanning calorimetry (DSC). The temperature of 5% weight loss was selected as the onset point of decomposition. As shown in Figures S9 and S10 (Supporting Information), all the polymers exhibited excellent stability with decomposition temperatures beyond 330 °C. We did not observe any thermal transition for these polymers from the differential scanning calorimetry analysis in the range of –20 to 300 °C.

Optical properties of all NDI-2Tz based polymers were measured by UV–vis-near-infrared absorption in dilute chloroform solution and thin film state, and the spectra are shown in Figure S13 (Supporting Information) with the corresponding parameters summarized in **Table 1**. All NDI-2Tz polymers exhibit a strong absorption in the range of 600–1000 nm in solution due to intramolecular charge transfer between the acceptor NDI unit and the donor dialkoxybithiazole unit. The less pronounced π–π^* transition absorption (300–500 nm) in the NDI-2Tz based polymers indicate the highly planar backbone. When going from solution to film, we observed no obvious redshifts for the λ_{max} peaks, indicating high backbone rigidity for these three copolymers, also confirmed by DFT calculation (Figure S10, Supporting Information). The band-tail absorption increases as the density of the EG side chain in thin films increases. Because of the higher density of the tri(ethylene glycol) side chains, the polarizability around the polymer backbone increases. This phenomenon can be regarded as the solid-state equivalent of solvatochromism, which affects

Table 1. Optical properties, electrochemical properties, energy levels, and water contact angle (θ) of the TEG series polymers.

Polymer	λ_{onset}, film [nm]	E_g opt.a) [eV]	HOMO b) [eV]	LUMO c) [eV]	E_{onset} ox.b) [V]	E_{onset} red.c) [V]	θ
0 TEG	1177	1.05	–5.81	–4.05	0.711	–1.049	104.2 ± 5.5
1 TEG	1238	1.00	–5.68	–4.24	0.581	–0.855	97.6 ± 1.0
2 TEG	1280	0.97	–5.63	–4.35	0.533	–0.746	83.3 ± 1.4

a)Optical bandgap calculated using the onset of the thin film absorption spectra ($E_g^{opt} = 1240/\lambda_{onset}$); b)Onset of CV oxidation recorded in a $CHCN_3$ solution containing Bu_4NPF_6 electrolyte. HOMO = – (5.10+ E_{onset} ox.) eV; c)Onset of CV reduction recorded in a $CHCN_3$ solution containing Bu_4NPF_6 electrolyte. LUMO = – (5.10+ E_{onset} red.) eV.

© 2022 The Authors. Advanced Functional Materials published by Wiley-VCH GmbH

the charge-transfer band.[35] Based on the thin film absorption onsets, the optical band gaps are calculated to be 1.05, 1.00, and 0.97 eV for 0 TEG, 1 TEG, and 2 TEG, respectively.

The cyclic voltammetry (CV) characterization of all NDI-2Tz based polymers was carried out to investigate the effects of TEG side-chain density on the energy level. As shown in Figure S12 (Supporting Information), all polymers exhibit distinctive reduction and oxidation peaks in a $CHCN_3$ solution containing 0.1 M Bu_4NPF_6 electrolyte. The highest occupied molecular orbital (HOMO) and the lowest unoccupied molecular orbital (LUMO) energy levels of these three polymers are calculated from the onset of oxidation and reduction potentials using the equation $E_{HOMO} = -(5.10 + E_{onset}^{ox.})$ eV and $E_{LUMO} = -(5.10 + E_{onset}^{red.})$ eV, respectively. The onset reduction potentials of 0 TEG, 1 TEG, and 2 TEG relative to the half-wave potential of ferrocene/ferrocenium (Fc/Fc^+) were –1.05, –0.86, and –0.75 V, respectively, which correspond to estimated LUMO energies of –4.05, –4.24, and –4.35 eV. The relatively deep LUMO levels are the result of the strong electron affinity of the acceptor monomer naphthalenediimide (NDI) and the electron-deficient nature of bithiazole (2Tz). The LUMO levels decrease with the density of the TEG side chain which indicates the glycol ethers have inductive effects on the electronic structure.[36,37] This was also verified by DFT calculations (Figure S10, Supporting Information). The onset oxidation potentials of 0 TEG, 1 TEG and 2 TEG relative to Fc/Fc^+ redox were 0.71, 0.58, and 0.53 V, respectively, which correspond to estimated HOMO energies of –5.81, –5.68, and –5.63 eV. The increased HOMO energy level also benefits the hole transport, which results in ambipolar OECT operation.

2.2. Aqueous Electrolyte Gated OECTs

Following polymer synthesis and characterization, we fabricated OECTs by employing interdigitated electrodes as source and drain (channel length of 5 um, MicruX technologies) and using these polymers as the channel material and evaluated their OECT performance, as illustrated in **Figure 2**. The conjugated polymers were deposited by spin coating using chloroform as a solvent without additives or further annealing steps. The device fabrication details are provided in the supporting information. We subsequently investigated the device performance employing an aqueous 100 mM NaCl solution electrolyte and an Ag/AgCl gate electrode. The transfer characteristics of these polymers are shown in Figure 2b and the corresponding OECT parameters are summarized in **Table 2**. Both 1 TEG and 2 TEG exhibit ambipolar OECT character with n-type dominated performance and increasing current with increasing V_G indicating that the devices operate in accumulation mode. The solely alkyl chain substituted polymer 0 TEG is unable to be gated (i.e., no turn-on current when applying gate voltage). 2 TEG, which has the highest density of TEG side chains, exhibits the highest on-current among these three polymers. A detailed comparison between 1 TEG and 2 TEG in OECT performance is presented in Figure 2c–h. 2 TEG exhibits a large on-off ratio close to 10^5 (9.2×10^4, Figure 2f) while 1 TEG displays $\approx 10^4$ ratio (Figure 2c) in semi-log transfer curves, compared with NDI-bithiophene based polymers that have a reported on-off ratio of $\approx 10^3$,[38] and BBL which has an on-off ratio of 6×10^3.[20] The maximum transconductance of 2 TEG based OECTs is attained at a V_G of 0.8 V with an average value of 51.8 mS, which is four times higher than that of 1 TEG (average value of 12.3 mS, at $V_G = 0.8$ V). 1 TEG shows a much larger hysteresis in both transfer and output curves (Figure 2c,d) than 2 TEG (Figure 2f,g), indicating that ion motion in 1 TEG is much slower than in 2 TEG. To evaluate the response speed of 1 TEG and 2 TEG OECTs, the transient response time of 1 TEG is extracted by an exponent fit to the source-drain current under pulsed gate voltage in Figure 2e. 1 TEG is slow with time constants $\tau_{on/off} = 5.7/0.56$ s for ON and OFF. 2 TEG switches on and off in <100 ms (Figure 2h, the measurement is out of instrument resolution and therefore cannot be fitted).

To gain insight into the differences in performance of the polymers in OECTs, we investigated the influence of the side chains on the non-fused NDI-2Tz polymers' wettability, electrochemical properties, and molecular packing. Being able to interact with electrolytes is essential for OECTs and thus the wettability of the polymer film is critical for ion penetration and transport. The hydrophilicity of the polymers is studied by water contact angle (Figure S12, Supporting Information), indicating that the contact angle decreases as the amount of TEG side chains increases. The 2 TEG polymer has the highest amount of TEG side chains, featuring the best wettability that enables efficient ion diffusion and electrochemical doping, while 0 TEG has only hydrophobic alkyl side chains, which prevents ions to approach the conjugated polymer backbones for electrochemical doping and therefore cannot be gated.

We carried out Cyclic Voltammetry (CV) measurements of the polymers on indium tin oxide (ITO) in a 100 mM NaCl aqueous solution to investigate the effect of side-chain substitution on the reduction potential in film. As shown in **Figure 3**a, we clearly observed that the reduction onset potentials gradually shift from –0.30 V for 0 TEG to –0.29 V for 1 TEG to –0.17 V for 2 TEG, indicating that the most hydrophilic 2 TEG is easiest to be reduced electrochemically in aqueous electrolyte (doped by cations). The shift in reduction onset likely stems from the difference in electron affinity and ease of ion diffusion into the bulk film during electrochemical redox doping. The ion doping process of the polymer was monitored by spectroelectrochemistry measurements that were also carried out in the 100 mM NaCl aqueous solution. Here the films were electrochemically reduced and oxidized using an Ag/AgCl electrode (Figure 3; Figures S15 and S16, Supporting Information). Figure 3b,c show the absorbance spectra of 1 TEG and 2 TEG films in the reduced states at various bias potentials (from 0 to –0.9 V) displaying the reduced states. Upon increasing the reducing potential, the main neutral intramolecular charge transfer (ICT) absorption (around 950 nm) gradually diminishes while new absorbing species emerge at around 550 and 1200–1300 nm due to a polaronic (and/or bipolaronic) absorption. 2 TEG exhibits a higher ratio (polaronic/ICT absorption) than that of 1 TEG at a given bias, indicating a higher electrochemical doping efficiency due to the higher number of TEG side chains, improving the ion-penetration capability. No polaron generation was observed in the 0 TEG spectra (Figure S19, Supporting Information). These results confirm the importance of introducing TEG side chains to the polymer

© 2022 The Authors. Advanced Functional Materials published by Wiley-VCH GmbH

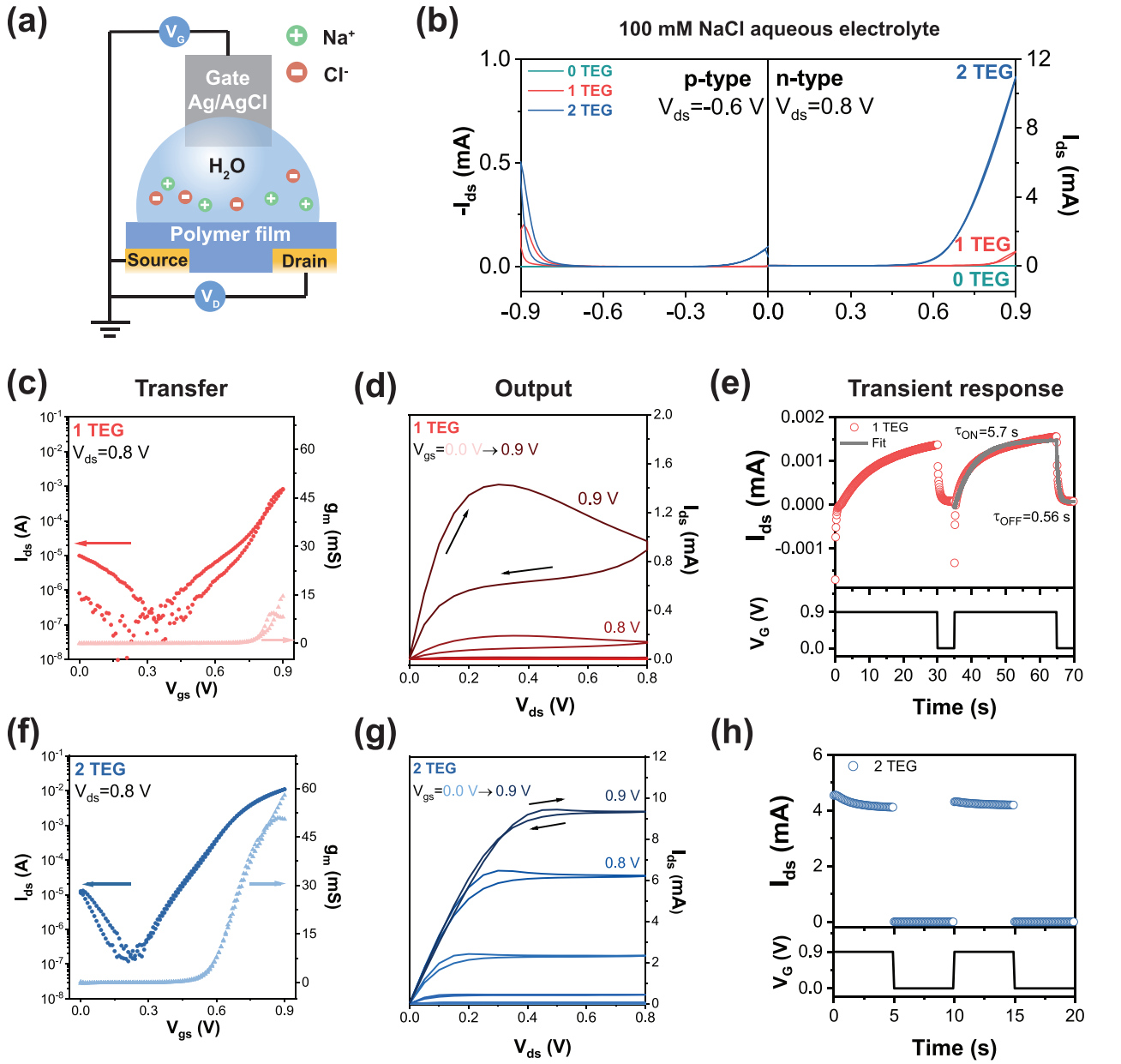

Figure 2. a) Cross-sectional schematic of OECT device. b) Comparison of OECT performance of the polymers with various number of TEG sidechains in 100 mM NaCl aqueous solution. Ambipolar linear transfer curves of 0 TEG, 1 TEG and 2 TEG. The on-current of OECTs increases with the hydrophilicity of the semiconducting polymers. Semi-log transfer curve of c) 1 TEG and f) 2 TEG. Output curve of d) 1 TEG and g) 2 TEG. Transient response of e) 1 TEG and h) 2 TEG.

backbone to enhance ion transport. The volumetric capacitance C^* is extracted from electrochemical impedance spectroscopy (EIS) in 100 mM NaCl aqueous solution (Figure S21, Supporting Information). The capacitance values are obtained from fits of EIS data to an equivalent circuit of $R_s(R_p \| C)$ at each potential. Only 2 TEG shows an increased capacitance with

Table 2. Aqueous electrolyte-gated OECT characteristics of the polymers.

Polymer	d [nm]	g_m [mS]	On/off	V_{Th} [V]	$\mu_e^{OECTa)}$ [cm^2 V^{-1} s^{-1}]	C^* [Fcm^{-3}]	μC^*[Fcm^{-1} V^{-1} s^{-1}]
PNDI2OD-2Tz	61.7±13.0	N/A	N/A	N/A	N/A	N/A	N/A
PNDIODTEG-2Tz	56.0±3.8	12.3±3.7	≈10^4	0.75	N/A	N/A	N/A
PNDI2TEG-2Tz	49.4±9.8	51.8±2.5	≈10^5	0.54	3.16×10^{-3}	≈367	1.16±0.28

[a)]Calculated from C* and μC*.

© 2022 The Authors. Advanced Functional Materials published by Wiley-VCH GmbH

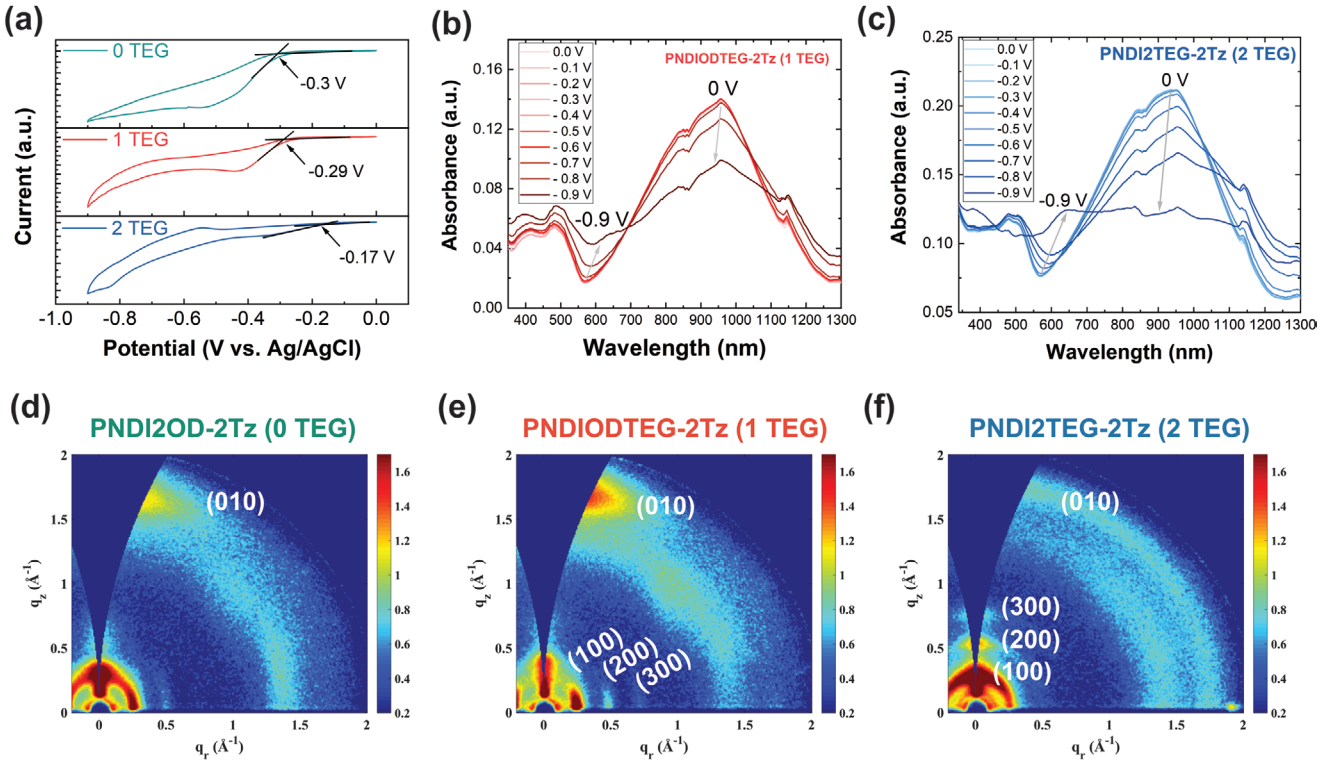

Figure 3. a) Cyclic voltammetry of polymer thin films (0 TEG, 1 TEG, and 2 TEG) on ITO substrates in 100 mM NaCl aqueous solution with the negative potential (reduction, n-type doping, scan rate 20 mV s^{-1}). Electrochemical spectroscopy of b) 1 TEG and c) 2 TEG with the negative potential versus Ag/AgCl in 100 mM NaCl aqueous solution (reduction, n-type doping). 2D GIWAXS patterns of d) 0 TEG, e) 1 TEG, and f) 2 TEG thin films.

applying potential, while 0 TEG and 1 TEG do not increase (resembling the bare gold electrode) (Figure S22, Supporting Information). The estimated C^* of 2 TEG is 367 F cm^{-3}, which is similar to the reported NDI-2T based polymers. The OECT electron mobility was calculated using $\mu C^* = 1.16$ F cm^{-1} V^{-1} s^{-1} (extracted from the slope of the linear fitting in the plot of g_m versus OECT channel geometry, Figure S29, Supporting Information) and measured C^*. The OECT mixed ionic and electronic charge carrier mobility of 2 TEG is calculated to be 3.16×10^{-3} cm^2 V^{-1} s^{-1}, which is on par with the well-performing n-type OECT polymers, like the NDI-thiophene based P-90[14] and BBL.[20] We next explore how the TEG side chains impact the charge mobility in non-fused NDI-2Tz backbone polymers. As previously shown in the literature,[14] introducing TEG side chains might result in a significant drop in electron mobility. We investigated the charge transport properties of pristine 0 TEG, 1 TEG, and 2 TEG using bottom contact/top gate field-effect transistors (Figure S17, Supporting Information). The field-effect electron mobility for 0 TEG, 1 TEG, and 2 TEG, was determined to be $\approx 10^{-2}$ cm^2 V^{-1} s^{-1} at room temperature. The reported 2 TEG field-effect mobility is 3.5×10^{-2} cm^2 V^{-1} s^{-1}.[35] Unfortunately, due to relatively high gate leakage currents, we are unable to determine the field-effect mobility accurately, though the order of magnitude remains the same, see Figure S17 (Supporting Information). The polymers exhibit the ambipolar properties both in OFETs and in OECTs (Figure S17, Supporting Information). These results indicate that non-fused NDI-2Tz backbone-based 2 TEG are able to achieve both high electron mobility and efficient ion transport properties at the same time, which is essential for effective OECT performance. The aqueous electrolyte-gated OECT is summarized in Table 2.

To understand how the TEG side chains influence the polymer film crystallinity and molecular packing and how this correlate to the device performance, grazing incidence wide-angle X-ray scattering measurements on polymer films were carried out. The results are shown in Figure 3d–f and Figure S23 (Supporting Information) includes the corresponding line cuts. Though all these polymers have the same NDI-2Tz backbone, replacing alkyl chains with TEG side chains results in significant differences in the microstructure and molecular packing. The 0 TEG chain shows a bimodal orientation with both face-on and edge-on fractions: a (100) peak at $q_{xy} = 0.25$ $Å^{-1}$ and (010) peaks at $q_z = 1.65$ $Å^{-1}$ and was observed together with a (100) peak at $q_z = 0.28$ $Å^{-1}$. On the contrary, both 1 TEG and 2 TEG chains tend to adopt monoidal orientation. 1 TEG shows a predominant face-on orientation with an improved crystallinity (compared with 0 TEG), exhibiting lamellar diffractions up to the third-order (300) at $q_{xy} = 0.71$ $Å^{-1}$ in the in plane (IP) direction together with the (010) peak at $q_z = 1.67$ $Å^{-1}$ in the out of plane (OOP) direction. 2 TEG appears to pack mostly with an edge-on orientation relative to the substrate, exhibiting lamellar diffractions progressing to the third order (300) at $q_z = 0.75$ $Å^{-1}$ in the IP direction together with an (010) peak at $q_z = 1.71$ $Å^{-1}$ in the OOP direction. This polymer further exhibits a preferential edge-on oriented molecular packing, which is known to be favorable for charge carrier transport in OFET devices. Based on the (010) diffraction, the π–π stacking was calculated to be 3.81 Å for 0 TEG, 3.76 Å for 1 TEG, and 3.67 Å for 2 TEG,

© 2022 The Authors. Advanced Functional Materials published by Wiley-VCH GmbH

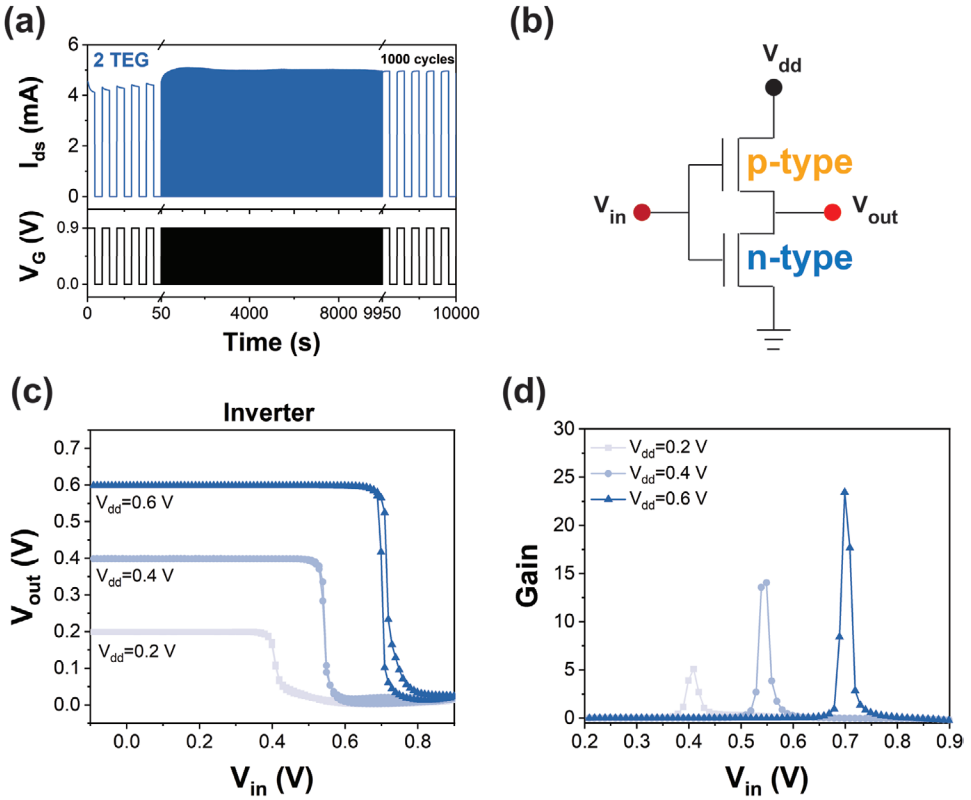

Figure 4. a) Operation stability measurement of 2 TEG OECT. 1000 pulse cycles of Drain current (I_{ds}) were monitored when a gate voltage pulse $V_G = 0.9$ V was applied for 5 s with an interval time of 5 s ($V_{ds} = 0.6$ V). b) The schematic of the inverter c) The complementary inverter input-output characteristics using Pg2T-TT as p-type channel and 2 TEG as n-type channel, 100 mM NaCl as electrolyte. d) The corresponding inverter gain ($|\partial V_{out}/\partial V_{in}|$).

respectively, showing gradual reduced distance with increased amounts of TEG side chains. We also calculated the crystal coherence lengths (CCLs) to be 24.74 Å for 0 TEG, 28.82 Å for 1 TEG, and 33.60 Å for 2 TEG, respectively, implying the crystallinity is enhanced. The increased crystallinity and preferential edge-on orientation of 2 TEG are the main contributing factors to the improved charge carrier transport in OECT and OFET devices.

To assess device operation performance, stability is a key factor that needs to be taken into account for successful applications. **Figure 4**a shows the stability of n-type drain current (V_{ds} = 0.6 V) upon consecutive gate voltage pulsing (5 s with $V_G = 0.9$ V and 5 s of delay). The device was stable, and no degradation was observed until 1000 cycles. The on current decreases to ≈25% after 4000 cycles, but still displays the same on-off ratio (Figure S33a, Supporting Information). The device eventually broke down at the 4887th cycle (Figure S33, Supporting Information). Reproducibility of individual device performance is essential for integrated circuits and arrays. We repeated the OECT characterization measurements on different devices (as well as with different dimensions of interdigitated microelectrodes), and we find almost no variation among devices (Figure S30, Supporting Information). The 2 TEG based OECTs can also operate in phosphate buffered saline (PBS) (Figure S30a, Supporting Information), which has the potential for bio-applications like metabolite sensing.[12] Additionally, we performed a shelf-life stability test where the devices were stored in ambient condition. Even though the current degraded by over 40% after 1 month, the current remains at a ≈mA magnitude (Figure S31, Supporting Information). In fact, only a very minor decrease in the on-off ratio is observed, which is still over 10^4 for all four devices (Figure S32, Supporting Information). We combined our n-type 2 TEG based OECT with a p-type Pg2T-TT based OECT to form an inverter for logic circuits often used as an amplifier for biosignals[39] (see Figure 4b). The inverter shows small hysteresis and a maximum gain ($|\partial V_{out}/\partial V_{in}|$) of 23.4 at V_{dd} = 0.6 V (see Figure 4c,d). We also show the aqueous OECT operation of 2 TEG using devices made with lithography and parylene liftoff[40] (Figure S35, Supporting Information). In general, we find that TEG side chains improve the OECTs performance with respect to the on-off ratio, transconductance, and operation speed by facilitating ion transport and ion coupling while introducing the nitrogen to the polymer backbone improves electron mobility. Together these two factors make for the high operating performance of the 2 TEG in aqueous electrolyte-gated OECTs.

2.3. Ion Gel Gated Electrochemical Transistors and Resistive Random-Access Memory Devices (EC-RAMs)

To demonstrate the versatility of the material, we also investigated ionic liquid-gated electrochemical devices. Ionic liquids are used in electrolyte-gated transistors because they

© 2022 The Authors. Advanced Functional Materials published by Wiley-VCH GmbH

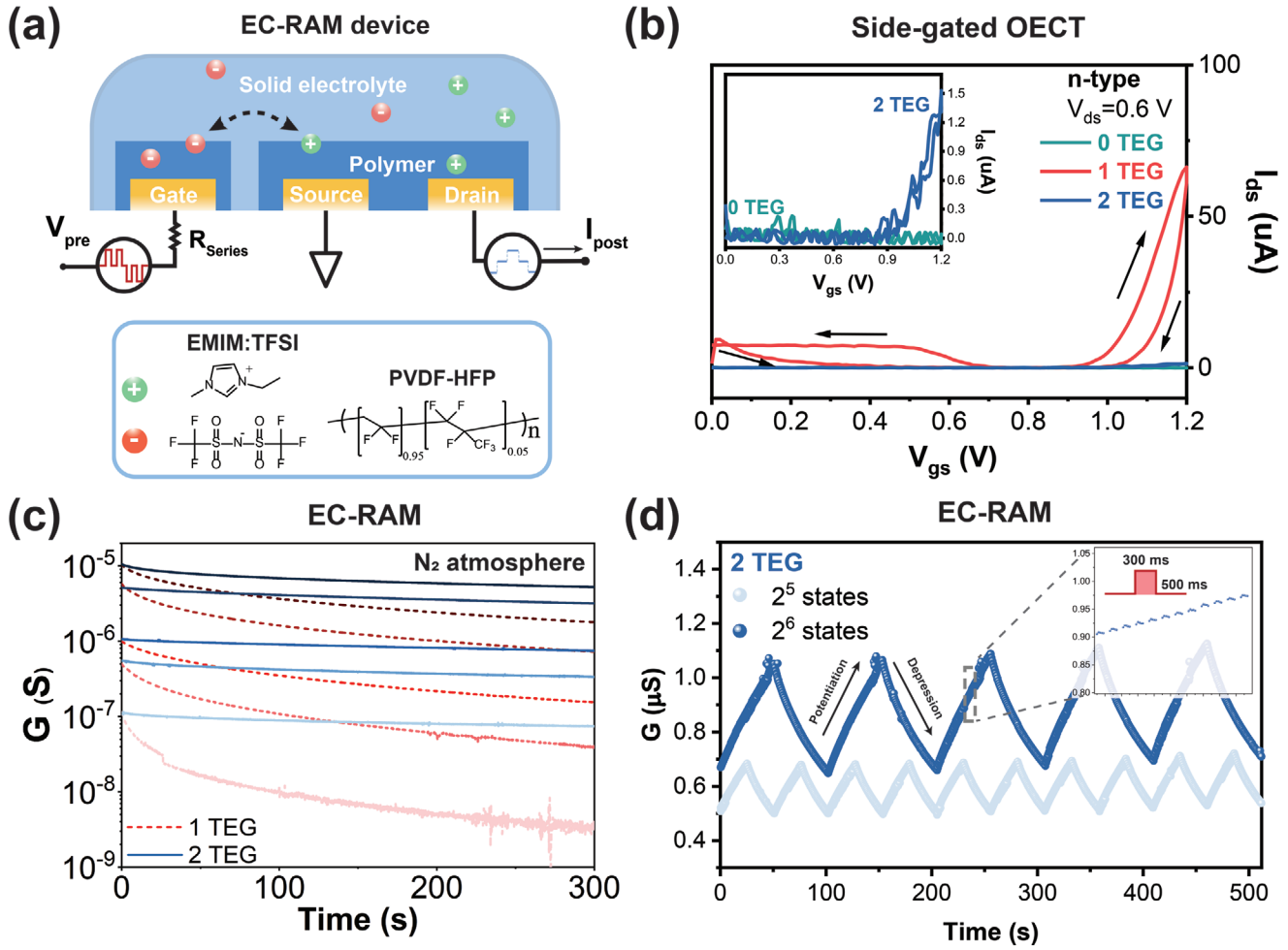

Figure 5. a) Schematic of the ion gel side-gated EC-RAMs including chemical structures of the ionic liquid (EMIM:TFSI) and PVDF-HFP. b) Linear transfer curves of 0 TEG, 1 TEG, and 2 TEG measured in ambient conditions (scan rate 10 mV s^{-1}). c) The state retention of 1 TEG and 2 TEG over 5 min while the gate is in open circuit. Measured in a nitrogen atmosphere. d) 2 TEG EC-RAM linear potentiation and depression programming individually with 32 or 64 conductance states (pulse width 300 ms and delay time 500 ms with a 1 GOhm series resistor. +10 V for potentiation and –3 V for depression). Measured in a nitrogen atmosphere.

have a larger electrochemical window compared to water,[41] a high capacitance, and can be printed.[42] Moreover, it has been previously reported that water can introduce traps in organic semiconductors and hinder OFETs performance during operation.[43–45] The ionic liquid—1-ethyl-3-methylimidazolium bis(trifluorosulfonyl)imide (EMIM:TFSI)—is blended with poly(vinylidene fluoride-co-hexafluoropropylene) to prepare the ion gel solid electrolyte, as described in previous reports.[46] For ion gel gating we adopted a side gate architecture, which simplifies fabrication using lithography. **Figure 5**a shows the schematic of the organic electrochemical resistive random-access memory devices (EC-RAMs), which are also able to operate as conventional side-gated OECTs. The device microscope image is shown in Figure S37 (Supporting Information). We first characterized the ion gel gated OECTs performance of 0 TEG, 1 TEG, and 2 TEG in ambient conditions. The n-type OECT transfer characteristic of these three polymers is shown in Figure 5b. 1 TEG shows the highest on-current among the three polymers, while no source-drain current is measured in 0 TEG devices (similar to aqueous electrolyte gating). The on-off ratio of 1 TEG is about two orders of magnitudes higher than 2 TEG in both p- and n-type transfer curves shown in Figure S39 (Supporting Information). 1 TEG polymer film shows larger porous structures in the AFM image (Figure S18, Supporting Information), which we speculate is to allow the large ionic liquid ions (larger than Na^+ and Cl^-) to penetrate the polymer film easier, resulting in enhanced doping efficiency. Both 1 TEG and 2 TEG exhibit ambipolar properties, like in the aqueous electrolyte case (shown in Figures S38 and S39, Supporting Information). EC-RAMs typically operate at a low voltage and display numerous accessible non-volatile conductance states.[7] These conductance states could be implemented as synaptic weights in hardware-based artificial neural networks (ANNs). For these networks state retention is important.[47] We compared 1 TEG and 2 TEG based EC-RAM state retention over time in n-type mode (positive drain and gate voltage) when the gate is in an open circuit (shown in Figure 5c). The conductance states of 2 TEG show good state retention in all conductance ranges in the nitrogen atmosphere. 2 TEG exhibits 50%

© 2022 The Authors. Advanced Functional Materials published by Wiley-VCH GmbH

decrease in the conductance at a level of 10^{-5} S while that of 1 TEG decays over 80% in 5 min. At a low conductance level of 10^{-7} S, 1 TEG decays over an order of magnitude in 5 min, and 2 TEG decays <30% while remaining in the same order of magnitude. The state retention indicates that 2 TEG is better equipped to hold the cations and prevent the cation diffusion back to the electrolyte than 1 TEG. We hypothesize that TEG chains coordinate (or crown) cations such that the rate of their exfiltration from the film is inversely proportional to the density of TEG chains. Hardware-based ANNs (like parallel arrays) require that the accessible conductance states of each EC-RAM is linearly programable by external write voltages.[48] Meanwhile, each state should be distinguishable. The linear programming cycles of 2 TEG based EC-RAM with 32 and 64 potentiation and depression steps are shown in Figure 5d. As illustrated in Figure 5a, a series resistor is used to control the gate current and prevent the loss of the conductance state.[49] A voltage pulse (amplitude +10 V for potentiation and –3 V for depression, width of 300 ms) is applied at the gate. The inset is a zoom-in image clearly showing the individual conductance states during 500 ms. Although the number of required conductance states is hard to predict a priori, being strongly dependent on application, devices with 10–100 clearly distinct states often lead to sufficiently high ANN accuracy.[47] More importantly, the 2TEG EC-RAM allows for linear and symmetric programming, demonstrating its potential for neuromorphic computing applications. In summary, in ion gel gating, 1 TEG exhibits a higher on-off ratio than 2 TEG in transistor operation, while 2 TEG is a better candidate for EC-RAM applications based on the enhanced state retention. It is important to consider the application when designing a material and, for that, to understand the structure-property relationship. Currently, the mechanisms underlying the observed state retention of 1 TEG and 2 TEG remain unclear, requiring further investigation.

3. Conclusion

We have developed a series of non-fused, planar NDI-2Tz copolymers decorated with and without hydrophilic TEG side chains, and investigated their OECT performance in aqueous electrolyte and ionic liquid, as well as their EC-RAM performance. Compared to the non-TEG side-chain substituted or mono-TEG side-chain substituted polymers, the polymer with two TEG side chains (PNDI2TEG-2Tz, 2 TEG) exhibits the highest OECT performance in the merits of transconductance, μC^*, on-off ratio and operation speed in aqueous electrolyte, owing to improved ion conductivity and volumetric capacitance. In addition, benefiting from the highly planar and rigid backbone, favorable backbone orientation and low-lying LUMO energy level, PNDI2TEG-2Tz (2 TEG) achieved electron mobility up to 3.16×10^{-3} cm^2 V^{-1} s^{-1} in OECT and $\approx 10^{-2}$ cm^2 V^{-1} s^{-1} in OFET operation. Moreover, the double TEG chain substituted polymer exhibits good conductance state retention over 2 orders of magnitudes in electrochemical resistive random-access memory devices (EC-RAMs), highlighting its potential for neuromorphic computing. This work demonstrates that non-fused donor-acceptor conjugated polymers can achieve high electron mobility and ion penetration capability simultaneously, an essential characteristic for OECTs. The work contributes to a deeper understanding of the relationship between the polymer structure and the performance of n-type OECTs, opening a window toward designing even higher performance n-type OECT materials.

4. Experimental Section

Materials: The synthesis details of the NDI-2Tz based D–A copolymers are described in the Supporting Information. Chloroform, 1-ethyl-3-methylimidazolium bis(trifluorosulfonyl)imide, poly(vinylidene fluoride-co-hexafluoropropylene) are purchased from Sigma-Aldrich and used as received. The interdigitated microelectrodes IDA-Au-1, IDA-Au-5, IDA-Au-6 are purchased from MicruX technologies. The parameters of interdigitated microelectrodes are summarized in Table S3 (Supporting Information).

Device Fabrication and Characterizations: The polymer solutions were prepared in chloroform (5 mg mL^{-1}). The interdigitated microelectrodes were treated with UV ozone for more than 15 min, following spin-coating the polymer solutions at 1000 rpm for 30 s. For ion gel side gated devices, the Au gate electrode is placed next to the interdigitated electrodes. The polymers were spun cast on top, followed by laser ablation to separate the gate and the active channel. The ion gel electrolyte spans over the gap. The electrical characterization of OECTs is recorded by a Keithley sourcemeter 2602B, which is controlled by the software Arkeo developed by Cici research. The fabrication of patterned N-type polymer OECTs is described in the Supporting Information.

Cyclic Voltammetry (CV) and Electrochemical Impedance Spectroscopy (EIS): Cyclic voltammetry measurements were performed using a Biologic SP-150 potentiostat with a standard three electrodes configuration in 100 mM NaCl aqueous solution. Polymer thin films were spun on an ITO glass used as a working electrode, together with a platinum wire as the counter electrode and an Ag/AgCl electrode as the reference electrode. Electrochemical Impedance Spectroscopy was also performed with the three electrodes system in a 100 mM NaCl aqueous solution. The polymers were spun on SU-8 patterned 2.5 × 2.5 mm Au electrodes used as working electrode, together with a platinum wire as the counter electrode and an Ag/AgCl electrode as the reference electrode.

UV–vis-NIR Electrochemical Spectroscopy: The measurements were carried out following a previously reported method.[50] The polymer thin films were deposited on ITO glass, and then immersed into a cuvette which is filled with 100 mM NaCl aqueous electrolyte, together with Ag/AgCl electrode. The UV–vis-NIR transmission of polymer films was monitored in situ at different voltages (vs Ag/AgCl) to probe the neutral and charged states during electrochemical doping.

Film-Thickness Measurements: The thickness of spun polymer thin films was characterized by a Veeco Dektak 150 profilometer.

GIWAXS: Grazing incidence wide-angle X-ray scattering (GIWAXS) measurements were performed using a MINA X-ray scattering instrument built on a Cu rotating anode source (= 1.5413 Å). 2D patterns were collected using a Vantec500 detector (1024× 1024 pixel array with pixel size 136× 136 μm) located 122 mm away from the sample. The films were placed in reflection geometry at certain incident angles with respect to the direct beam using a Huber goniometer. GIWAXS patterns were acquired using incident angles from 0.2° in order to probe the thin film structure. The direct beam center position on the detector and the sample-to-detector distance were calibrated using the diffraction rings from standard silver behenate and Al_2O_3 powders.

Supporting Information

Supporting Information is available from the Wiley Online Library or from the author.

© 2022 The Authors. Advanced Functional Materials published by Wiley-VCH GmbH

Acknowledgements

Y.Z., E.R.W.v.D., and Y.v.d.B. gratefully acknowledge funding from the European Union's Horizon 2020 Research and Innovation Programme, grant agreement no. 802615. G.Y. and J.S. acknowledge the National Natural Science Foundation of China (61620106016/61835009/61775145). G.Y. also acknowledges the China Postdoctoral Science Foundation Funded Project (grant 2020M672771) and Guangdong Basic and Applied Basic Research Foundation (2020A1515110636). T.P.A.v.d.P. acknowledges funding from the Netherlands Ministry of Education, Culture and Science (Gravity program 024.001.035). G.P. acknowledges the Zernike Institute for Advanced Materials for the startup funds. J.D. and G.P. are grateful to the China Scholarship Council (CSC No. 201606340158). Y.v.d.B., I.K., and P.G. acknowledge funding for a joint project between the Max Planck Institute of Polymer Research and the Institute for Complex Molecular Systems (ICMS), Eindhoven University of Technology, grant no. MPIPICMS2019001.

Conflict of Interest

The authors declare no conflict of interest.

Data Availability Statement

The data that support the findings of this study are available from the corresponding author upon reasonable request.

Keywords

ethylene glycol side chains, neuromorphic devices, non-fused donor-acceptor conjugated polymers, organic electrochemical transistors

Received: February 9, 2022
Revised: March 22, 2022
Published online:

[1] J. Rivnay, S. Inal, A. Salleo, R. M. Owens, M. Berggren, G. G. Malliaras, *Nat. Rev. Mater.* **2018**, *3*, 17086.
[2] D. Khodagholy, J. Rivnay, M. Sessolo, M. Gurfinkel, P. Leleux, L. H. Jimison, E. Stavrinidou, T. Herve, S. Sanaur, R. M. Owens, G. G. Malliaras, *Nat. Commun.* **2013**, *4*, 2133.
[3] P. Andersson Ersman, R. Lassnig, J. Strandberg, D. Tu, V. Keshmiri, R. Forchheimer, S. Fabiano, G. Gustafsson, M. Berggren, *Nat. Commun.* **2019**, *10*, 5053.
[4] S. Inal, J. Rivnay, A.-O. Suiu, G. G. Malliaras, I. McCulloch, *Acc. Chem. Res.* **2018**, *51*, 1368.
[5] C. Cea, G. D. Spyropoulos, P. Jastrzebska-Perfect, J. J. Ferrero, J. N. Gelinas, D. Khodagholy, *Nat. Mater.* **2020**, *19*, 679.
[6] Y. van de Burgt, A. Melianas, S. T. Keene, G. Malliaras, A. Salleo, *Nat. Electron.* **2018**, *1*, 386.
[7] Y. van de Burgt, E. Lubberman, E. J. Fuller, S. T. Keene, G. C. Faria, S. Agarwal, M. J. Marinella, A. Alec Talin, A. Salleo, *Nat. Mater.* **2017**, *16*, 414.
[8] B. D. Paulsen, K. Tybrandt, E. Stavrinidou, J. Rivnay, *Nat. Mater.* **2020**, *19*, 13.
[9] H. Bronstein, C. B. Nielsen, B. C. Schroeder, I. McCulloch, *Nat. Rev. Chem.* **2020**, *4*, 66.
[10] E. Zeglio, O. Inganäs, *Adv. Mater.* **2018**, *30*, 1800941.
[11] H. Sun, X. Guo, A. Facchetti, *Chem* **2020**, *6*, 1310.
[12] A. M. Pappa, D. Ohayon, A. Giovannitti, I. P. Maria, A. Savva, I. Uguz, J. Rivnay, I. McCulloch, R. M. Owens, S. Inal, *Sci. Adv.* **2018**, *4*, eaat0911.
[13] A. Giovannitti, C. B. Nielsen, D. T. Sbircea, S. Inal, M. Donahue, M. R. Niazi, D. A. Hanifi, A. Amassian, G. G. Malliaras, J. Rivnay, I. McCulloch, *Nat. Commun.* **2016**, *7*, 13066.
[14] A. Giovannitti, I. P. Maria, D. Hanifi, M. J. Donahue, D. Bryant, K. J. Barth, B. E. Makdah, A. Savva, D. Moia, M. Zetek, P. R. F. Barnes, O. G. Reid, S. Inal, G. Rumbles, G. G. Malliaras, J. Nelson, J. Rivnay, I. McCulloch, *Chem. Mater.* **2018**, *30*, 2945.
[15] S. Wang, H. Sun, T. Erdmann, G. Wang, D. Fazzi, U. Lappan, Y. Puttisong, Z. Chen, M. Berggren, X. Crispin, A. Kiriy, B. Voit, T. J. Marks, S. Fabiano, A. Facchetti, *Adv. Mater.* **2018**, *30*, 1801898.
[16] S. Wang, D. Fazzi, Y. Puttisong, M. J. Jafari, Z. Chen, T. Ederth, J. W. Andreasen, W. M. Chen, A. Facchetti, S. Fabiano, *Chem. Mater.* **2019**, *31*, 3395.
[17] J. Surgailis, A. Savva, V. Druet, B. D. Paulsen, R. Wu, A. Hamidi-Sakr, D. Ohayon, G. Nikiforidis, X. Chen, I. McCulloch, J. Rivnay, S. Inal, *Adv. Funct. Mater.* **2021**, *31*, 2010165.
[18] A. Savva, D. Ohayon, J. Surgailis, A. F. Paterson, T. C. Hidalgo, X. Chen, I. P. Maria, B. D. Paulsen, A. J. PettyII, J. Rivnay, I. McCulloch, S. Inal, *Adv. Electron. Mater.* **2019**, *5*, 1900249.
[19] S. Wang, H. Sun, U. Ail, M. Vagin, P. O. Å. Persson, J. W. Andreasen, W. Thiel, M. Berggren, X. Crispin, D. Fazzi, S. Fabiano, *Adv. Mater.* **2016**, *28*, 10764.
[20] H. Sun, M. Vagin, S. Wang, X. Crispin, R. Forchheimer, M. Berggren, S. Fabiano, *Adv. Mater.* **2018**, *30*, 1704916.
[21] X. Chen, A. Marks, B. D. Paulsen, R. Wu, R. B. Rashid, H. Chen, M. Alsufyani, J. Rivnay, I. McCulloch, *Angew. Chem., Int. Ed.* **2021**, *60*, 9368.
[22] K. Feng, W. Shan, S. Ma, Z. Wu, J. Chen, H. Guo, B. Liu, J. Wang, B. Li, H. Y. Woo, S. Fabiano, W. Huang, X. Guo, *Angew. Chem.* **2021**, *133*, 24400.
[23] H. Huang, L. Yang, A. Facchetti, T. J. Marks, *Chem. Rev.* **2017**, *117*, 10291.
[24] X. Chen, Z. Zhang, Z. Ding, J. Liu, L. Wang, *Angew. Chem., Int. Ed.* **2016**, *55*, 10376.
[25] W. Wu, Y. Liu, D. Zhu, *Chem. Soc. Rev.* **2010**, *39*, 1489.
[26] X. Guo, A. Facchetti, T. J. Marks, *Chem. Rev.* **2014**, *114*, 8943.
[27] C. Liu, K. Wang, X. Gong, A. J. Heeger, *Chem. Soc. Rev.* **2016**, *45*, 4825.
[28] L. Shi, Y. Guo, W. Hu, Y. Liu, *Mater. Chem. Front.* **2017**, *1*, 2423.
[29] C. B. Nielsen, A. Giovannitti, D. T. Sbircea, E. Bandiello, M. R. Niazi, D. A. Hanifi, M. Sessolo, A. Amassian, G. G. Malliaras, J. Rivnay, I. McCulloch, *J. Am. Chem. Soc.* **2016**, *138*, 10252.
[30] A. Giovannitti, D.-T. Sbircea, S. Inal, C. B. Nielsen, E. Bandiello, D. A. Hanifi, M. Sessolo, G. G. Malliaras, I. McCulloch, J. Rivnay, *Proc. Natl. Acad. Sci. USA* **2016**, *113*, 12017.
[31] Y. Wang, E. Zeglio, H. Liao, J. Xu, F. Liu, Z. Li, I. P. Maria, D. Mawad, A. Herland, I. McCulloch, W. Yue, *Chem. Mater.* **2019**, *31*, 9797.
[32] R. K. Hallani, B. D. Paulsen, A. J. Petty, R. Sheelamanthula, M. Moser, K. J. Thorley, W. Sohn, R. B. Rashid, A. Savva, S. Moro, J. P. Parker, O. Drury, M. Alsufyani, M. Neophytou, J. Kosco, S. Inal, G. Costantini, J. Rivnay, I. McCulloch, *J. Am. Chem. Soc.* **2021**, *143*, 11007.
[33] S. Wang, H. Sun, T. Erdmann, G. Wang, D. Fazzi, U. Lappan, Y. Puttisong, Z. Chen, M. Berggren, X. Crispin, A. Kiriy, B. Voit, T. J. Marks, S. Fabiano, A. Facchetti, *Adv. Mater.* **2018**, *30*, 1801898.
[34] J. Liu, G. Ye, B. van der Zee, J. Dong, X. Qiu, Y. Liu, G. Portale, R. C. Chiechi, L. J. A. Koster, *Adv. Mater.* **2018**, *30*, 1804290.
[35] J. Liu, G. Ye, H. G. O. Potgieser, M. Koopmans, S. Sami, M. I. Nugraha, D. R. Villalva, H. Sun, J. Dong, X. Yang, X. Qiu, C. Yao, G. Portale, S. Fabiano, T. D. Anthopoulos, D. Baran, R. W. A. Havenith, R. C. Chiechi, L. J. A. Koster, *Adv. Mater.* **2021**, *33*, 2006694.

© 2022 The Authors. Advanced Functional Materials published by Wiley-VCH GmbH

[36] Y. Shin, H. Komber, D. Caiola, M. Cassinelli, H. Sun, D. Stegerer, M. Schreiter, K. Horatz, F. Lissel, X. Jiao, C. R. McNeill, S. Cimò, C. Bertarelli, S. Fabiano, M. Caironi, M. Sommer, *Macromolecules* **2020**, *53*, 5158.
[37] G. Ye, J. Liu, X. Qiu, S. Stäter, L. Qiu, Y. Liu, X. Yang, R. Hildner, L. J. A. Koster, R. C. Chiechi, *Macromolecules* **2021**, *54*, 3886.
[38] A. F. Paterson, A. Savva, S. Wustoni, L. Tsetseris, B. D. Paulsen, H. Faber, A. H. Emwas, X. Chen, G. Nikiforidis, T. C. Hidalgo, M. Moser, I. P. Maria, J. Rivnay, I. McCulloch, T. D. Anthopoulos, S. Inal, *Nat. Commun.* **2020**, *11*, 3004.
[39] R. B. Rashid, W. Du, S. Griggs, I. P. Maria, I. McCulloch, J. Rivnay, *Sci. Adv.* **2021**, *7*, eabh1055.
[40] D. A. Koutsouras, T. Prodromakis, G. G. Malliaras, P. W. M. Blom, P. Gkoupidenis, *Adv. Intell. Syst.* **2019**, *1*, 1900013.
[41] M. Galiński, A. Lewandowski, I. Stępniak, *Electrochim. Acta* **2006**, *51*, 5567.
[42] S. H. Kim, K. Hong, W. Xie, K. H. Lee, S. Zhang, T. P. Lodge, C. D. Frisbie, *Adv. Mater.* **2013**, *25*, 1822.
[43] G. Zuo, M. Linares, T. Upreti, M. Kemerink, *Nat. Mater.* **2019**, *18*, 588.
[44] P. A. Bobbert, A. Sharma, S. G. J. Mathijssen, M. Kemerink, D. M. de Leeuw, *Adv. Mater.* **2012**, *24*, 1146.
[45] H. F. Iqbal, Q. Ai, K. J. Thorley, H. Chen, I. McCulloch, C. Risko, J. E. Anthony, O. D. Jurchescu, *Nat. Commun.* **2021**, *12*, 2352.
[46] K. H. Lee, M. S. Kang, S. Zhang, Y. Gu, T. P. Lodge, C. D. Frisbie, *Adv. Mater.* **2012**, *24*, 4457.
[47] A. Gumyusenge, A. Melianas, S. T. Keene, A. Salleo, *Annu. Rev. Mater. Res.* **2021**, *51*, 47.
[48] E. J. Fuller, S. T. Keene, A. Melianas, Z. Wang, S. Agarwal, Y. Li, Y. Tuchman, C. D. James, M. J. Marinella, J. J. Yang, A. Salleo, A. A. Talin, *Science* **2019**, *364*, 570.
[49] Y. Li, T. P. Xiao, C. H. Bennett, E. Isele, A. Melianas, H. Tao, M. J. Marinella, A. Salleo, E. J. Fuller, A. A. Talin, *Front. Neurosci.* **2021**, *15*, 636127.
[50] B. D. Paulsen, R. Wu, C. J. Takacs, H.-G. Steinrück, J. Strzalka, Q. Zhang, M. F. Toney, J. Rivnay, *Adv. Mater.* **2020**, *32*, 2003404.

© 2022 The Authors. Advanced Functional Materials published by Wiley-VCH GmbH